energy&fuels

Article

pubs.acs.org/EF

Preparation and Catalytic Activity of Thermosensitive Ga_2O_3 Nanorods

Vijay Bhooshan Kumar,[†,‡] Rahul Kumar Mishra,[†,‡] Indra Neel Pulidindi,[‡] Ze'ev Porat,[§,∥] John H. T. Luong,[⊥] and Aharon Gedanken*[,‡]

[‡]Bar-Ilan Institute for Nanotechnology and Advanced Materials, Department of Chemistry, Bar-Ilan University, Ramat-Gan 5290002, Israel

[§]Institute for Applied Research, Ben-Gurion University of the Negev, Be'er Sheva 84105, Israel

[∥]Division of Chemistry, Nuclear Research Center Negev, Be'er Sheva 84190, Israel

[⊥]Innovative Chromatography Group, Irish Separation Science Cluster (ISSC), Department of Chemistry and Analytical and Biological Chemistry Research Facility (ABCRF), University College Cork, Cork, Ireland

Supporting Information

ABSTRACT: Gallium oxide (β-Ga_2O_3) nanorods were prepared by ultrasonic irradiation of molten gallium in warm water to form α-GaO(OH). This precursor was then subjected to calcination in air at 600 °C for 3 h to form β-Ga_2O_3, as confirmed by X-ray diffraction (XRD). Field emission scanning electron microscopy (FE-SEM)/high-resolution transmission electron microscopy (HRTEM) micrographs revealed the formation of well-organized nanotubes/nanorods with homogeneous size distribution. The average length of the β-Ga_2O_3 nanorods was affected by the temperature of the water during sonication, decreasing from 480 to 72 nm with an increase in the temperature from 25 to 50 °C. A sharp decline in the particle size was also observed when the temperature was above 35 °C. The catalytic activity of the β-Ga_2O_3 nanorods was examined, as a model, during the dehydration reaction of xylose to furfural. Furfural is a versatile biomass-derived platform compound used for the synthesis of several strategic chemicals. This nanoscale catalyst has a large surface area, which enhances its catalytic activity and enables it to completely convert xylose to furfural at 150 °C within 12 h without any trace of byproducts, as confirmed by high-performance liquid chromatography (HPLC), ^{13}C nuclear magnetic resonance (NMR), and ^{1}H NMR. The XRD pattern of the used β-Ga_2O_3 nanorods was identical to that of pristine Ga_2O_3, indicating the possible reusability of this catalyst. β-Ga_2O_3 was reused for more reduction cycles, with similar results to the freshly prepared β-Ga_2O_3. HPLC analysis demonstrated that the selectivity of furfural is up to 94% compared to the 30% obtained with GaO(OH) as a catalyst.

1. INTRODUCTION

Nanoscale metals and nanosized metal oxides (MOs) exhibit unique physicochemical properties, functionality, and biocompatibility for a plethora of applications, including photonics, sensors, and catalysis.[1−3] Of particular interest is gallium oxide (Ga_2O_3), a chemically and thermally stable semiconductor with a wide bandgap of 4.9 eV. Its photocatalytic activity has been examined for water splitting, CO_2 photoreduction, and wastewater treatment.[4] Other applications include gas sensing,[5,6] photocatalysis,[7] optoelectric devices,[4] and polarized X-ray absorption imaging.[8] Ga_2O_3 also acts as an insulating barrier for spin-dependent tunneling junctions.[9] Its precursor GaO(OH) is also an effective photocatalyst, similar to the popular and effective TiO_2. The hydrothermal reaction of gallium with water at various temperatures has been reported for the synthesis of α-GaOOH in the presence of oxalic acid.[10]

The dehydration reaction of GaO(OH) into Ga_2O_3 occurs at elevated temperatures[4,11,12] via various synthetic routes: ball milling,[13] microwave treatment,[14] and the sonochemical reaction[15] of gallium.[3,6−8] Ga_2O_3 has several morphologies, depending upon the preparation procedure. For instance, the laser ablation method provides GaO(OH) of spindle-like and nanofiber form, which produces Ga_2O_3 nanorods upon dehydration.[11] A combined procedure of laser ablation followed by reflux in the presence of cetyltrimethylammonium bromide or polyvinylpyrrolidone produces a mixture of GaO(OH) and Ga_2O_3 nanowires.[16]

In the design of surface-exposed polymer−MO core−shell species, the core−shell must be easily accessed by the surrounding medium, a prerequisite for catalysis and sensing applications.[17−20] Stimuli- and thermoresponsive gallium-based oxides have been used as anchors for metal nanoparticles (NPs).[18] However, aggregation often compromises the performance of MO NPs. Therefore, the development of a convenient way to control the density of MO NPs with high precision is of uttermost importance.

The current research focuses on two main strategies: (a) the use of a heterogeneous as well as a selective acid catalyst and (b) the improvement of the process of furfural production from xylose. Solid catalysts are most often used because they show potential for advancement beyond current state-of-the-art methods. Moreover, they can be easily separated via simple filtration. The catalysts must display surface acidity, product selectivity through textural property adjustment, and enhanced

Received: June 30, 2016
Revised: August 8, 2016
Published: August 8, 2016

DOI: 10.1021/acs.energyfuels.6b01568
Energy Fuels 2016, 30, 7419−7427

Table 1. Summary of the Literature Reports on the Production of Furfural from Xylose Using Various Catalysts

type of catalyst/method for furfural production	solvent/catalyst	reaction conditions (time/temperature)	furfural yield (%)	reference
homogeneous/microwave	HCl + NaCl/$FeCl_3$ in water	15 min, 200 °C	90	26
homogeneous/hydrothermal	H_2SO_4, NaCl/$FeCl_3$ in water/toluene atmospheric pressure (boiling)	5 h, 170−185 °C	83	29
homogeneous/hydrothermal	biphasic organic/SO_3H^- acid ionic liquid	1 h, 100 °C	85	30
homogeneous/hydrothermal	EMIM/H_2SO_4 [1-ethyl-3-methylimidazolium hydrogen sulfate ([EMIM][HSO_4])] in water/toluene	6 h, 180 °C	84	27
hetrogeneous/hydrothermal	water/toluene; H-faujasite Si/Al = 15	6 h, 170 °C	90−95	31
hetrogeneous/hydrothermal	mixed solvents (water/dimethyl sulfoxide/tetrahydrofuran); β zeolite	6 h, 200 °C	42	32
hetrogeneous/hydrothermal	water, dimethyl sulfoxide (DMSO), and a mixture of water and toluene (water/toluene); H-zeolites	4 h, 140 °C	25	33
hetrogeneous/hydrothermal	water/toluene; layered zeolite Nu-6(1)	4 h, 170 °C	47	34
hetrogeneous/hydrothermal	water/toluene; Zr−W−Al mesoporous nanoparticles	2 h, 170 °C	50	35
hetrogeneous/microwave	water; ZrO_2−TiO_2	5 min, 300 °C	10	36
hetrogeneous/microwave	water/toluene; TiO_2−graphene oxide	10 min, 170 °C	68	37
hetrogeneous/hydrothermal	water; β-Ga_2O_3	12 h, 170 °C	94 selectivity (66 wt %)	current study

hydrothermal stability.[21] The most studied solid acids are zeolites,[22] which are highly crystalline microporous inorganic aluminosilicates, containing channels with well-defined pores of 0.5−1.3 nm, in which the catalytic groups are located.[23,24] Zeolites based on aluminosilicate are strong acidic catalysts and show excellent thermal and chemical stability.[23,24] Branca et al. reported the acidic pyrolysis of corncobs for furfural production at 800 K in a packed-bed reactor using several catalysts, such as H_2SO_4, H_3PO_4, H_3BO_3, $(NH_4)_2SO_4$, $ZnCl_2$, $NiCl_2$, $MgCl_2$, and $Fe_2(SO_4)_3$. The maximum yield of furfural production was 10%.[25] Marcotullio et al. studied the conversion of D-xylose to furfural in a solution of 50 mM HCl and NaCl at 200 °C, with 90% yield. They mentioned that the Cl^- ions promote the formation of 1,2-enediol from the acyclic form of xylose.[26] Lima et al. found that the combination of 1-ethyl-3-methylimidazolium hydrogen sulfate ionic liquids and H_2SO_4 provides the highest furfural yield of 85% from xylose at 180 °C.[27] However, the drawback of these methods is their inability to recycle the catalyst.[26,27] Recently, Mandalika et al. reported a reactive distillation batch process to produce furfural in excess of 85% of the theoretical yield based on pentose.[28] Ga_2O_3 was not used in any of the previous reports as a catalyst for the conversion of xylose to furfural. However, some other catalysts were used for this reaction, as listed in Table 1.

The catalysts in Table 1 are representative examples from literature reports. It is worth noting that most of the published work on the conversion of xylose to furfural is based on the use of ionic liquids, zeolite-based materials, and MOs.

Furfural is a versatile biomass-derived platform compound for the synthesis of several strategic chemicals, which are currently derived from petroleum.[38−41] Xylose, obtained from the hydrolysis of hemicellulose, is an abundant and underutilized substrate. The conversion of pentose sugars to value-added products is still a key pending issue in biorefinery. In the current work, we describe a facile and efficient sonochemical pathway for the preparation of Ga_2O_3 nanorods from molten Ga metal. The combined sonication and calcination techniques shorten the duration of the catalyst preparation (6 h) compared to conventional wet impregnation techniques. The β-Ga_2O_3 catalyst exhibits good activity and selectivity for the conversion of xylose to furfural. This solid catalyst can be easily separated from the product and reused. A proposed mechanism for the conversion of xylose to furfural is given.

2. EXPERIMENTAL SECTION

2.1. Chemicals. Metallic gallium (99.999%) was purchased from Aldrich and used as received, and xylose and furfural were obtained from Sigma-Aldrich, Israel. Doubly distilled water (DDW) obtained from a TREION purification system was used in this work.

2.2. Experimental Design and Methods. The detailed ultrasonic formation of Ga particles in aqueous media was reported elsewhere.[15,42−44] In brief, Ga_2O_3 was prepared by immersing a granule of Ga (ca. 1.0 g) in ∼20 mL of DDW, which was heated to 60 °C, forming a liquid gallium phase at the bottom of the test tube. The system was irradiated for 3 h with ultrasonic energy at 65% amplitude [ultrasonic transducer model VCX 750, Sonics & Materials, Newtown, CT, performed at 20 kHz and 230 V alternating current (AC)], giving a white-gray suspension, which turned into white flakes as the sonication proceeded. The resulting product was separated by centrifugation, dried in vacuum, and calcined at 600 °C under an ambient atmosphere in a muffle furnace. The conversion of xylose to furfural by Ga_2O_3 was performed at 150 °C for 12 h with a catalyst/xylose ratio of 1:1 (wt %). The reaction products were analyzed by ^1H and ^{13}C nuclear magnetic resonance (NMR) [300 MHz NMR (Bruker)] and a high-performance liquid chromatography (HPLC) chromatogram. The catalytic reactions were performed in water using a Teflon-lined stainless-steel autoclave [100 mL, stainless-steel autoclaves with a polytetrafluoroethylene (PTFE) hydrothermal synthesis reactor (MH-25) liner made in China] that contained a known amount of xylose (0.5−1 g) and Ga_2O_3 (0.05−0.5 g) and 20 mL of distilled water. A hydrothermal treatment was carried out for 2−12 h in the temperature range of 120−150 °C. The experimental conditions (reaction duration and temperature and the xylose/catalyst ratio) were varied to find the best furfural yield. The time was measured starting from the point at which the temperature of the mixture reached the set value. At a certain point in time, the reaction

DOI: 10.1021/acs.energyfuels.6b01568
Energy Fuels 2016, 30, 7419−7427

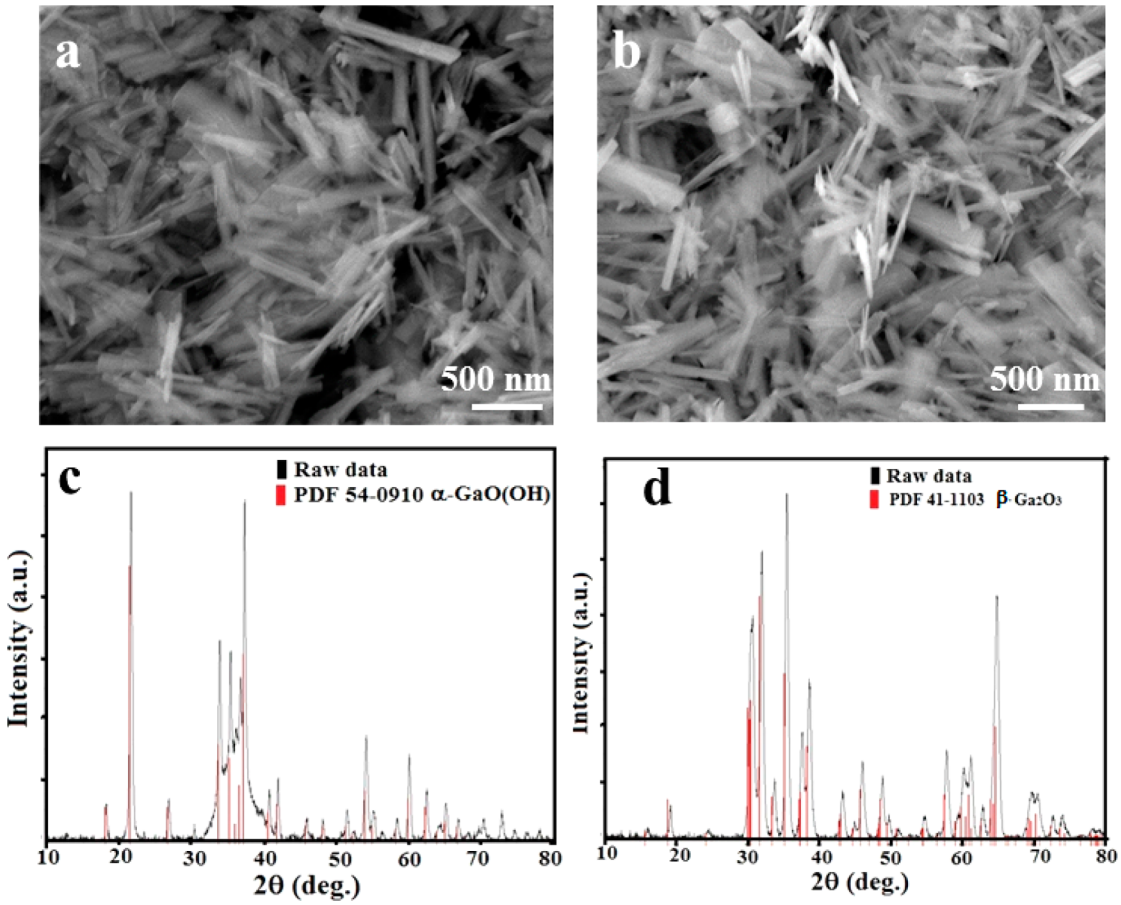

Figure 1. SEM micrograph of (a) α-GaO(OH) and (b) β-Ga_2O_3, (c) XRD of α-GaO(OH), and (d) XRD of β-Ga_2O_3.

was quenched by cooling the autoclave in a water bath. Time-dependent profiles were obtained by collecting the reaction results at different time points. The reaction mixture was centrifuged at 8000 rpm for 10 min at 15 °C, to separate the supernatant from the precipitate.

2.3. Analysis. Scanning electron microscopy (SEM) was performed using an Inspect FEI microscope. The samples were prepared by placing a small portion of the dried particles on a sample holder coated with carbon tape. For environmental scanning electron microscopy (ESEM) analysis, the sample surfaces were coated with a thin evaporated carbon layer for conductivity. Transmission electron microscopy (TEM) was performed using Tecnai G2, FEI, high contrast/cryo-TEM, (Hillsboro, OR), equipped with a bottom charge-coupled device (CCD) camera, 1000 × 1000. For TEM imaging, the particle-containing sample was dispersed in isopropanol and subjected to bath sonication. Three small droplets from the resulting suspension were then applied to a carbon-coated copper TEM grid and dried under vacuum in a covered Petri dish. Ultraviolet−visible (UV−vis) and diffusion reflectance spectra of materials were measured using a Cary 100 spectrophotometer (Varian), operated by Lab Sphere software. A Bruker D8 Advance and a Philips PW1050 X-ray diffractometer (Cu Kα radiation, operating at 40 kV/30 mA with a 0.0019 step size and a 0.5 s step) were used for X-ray diffraction (XRD). HPLC analysis was carried out on a Merch-Hitachi LaChrom system L-7000 equipped with a L-7455 diode array detector and a Schambeck SFD R1 2000 refractive index detector, Bad Honnef, Germany, using a 300 × 7.8 mm Rezex-ROA ion-exclusion chromatography column (Torrance, CA) equipped with a matching guard column.

3. RESULTS AND DISCUSSION

3.1. Formation of GaO(OH) and Characterization of α-GaO(OH) and β-Ga_2O_3. The ultrasonic irradiation induced acoustic cavitation in water, causing the dispersion of molten gallium into micrometric spheres. Under irradiation, the gallium spheres turned into white crystallites of GaO(OH) via the reaction of the gallium particles with dissolved oxygen and $OH^{\bullet}$ radicals that were formed by the partial decomposition of water.[15]

SEM images show that the α-GaO(OH) crystallites are shaped as nanorods (Figure 1a), ca. 500−1000 nm long and ca. 50−100 nm wide. Their composition and crystallinity are confirmed by XRD analysis (Figure 1c). Sharp intense signals from the crystal planes, typical of orthorhombic GaO(OH), are observed (Figure 1c). The dominant peaks are reflections of the (110), (130), (111), and (240) planes at the 2θ angles of 21.5°, 33.7°, 37.2°, and 54.02°, respectively. The crystallite sizes of GaOOH and Ga_2O_3 are calculated using Scheerer's equation and are found to be 17 and 18 nm, respectively. The density of the crystallites increases with the increase in sonication time (Figure S1 of the Supporting Information). Heating the α-GaO(OH) crystallites to 600 °C does not induce changes in their shape (Figure 1b) but rather in their chemical composition. The XRD pattern matches crystalline β-Ga_2O_3 (Figure 1d) with its monoclinic phase [Joint Committee on Powder Diffraction Standards (JCPDS) 41-1103]. The crystal structures of α-GaO(OH) and β-Ga_2O_3 were calculated on the basis of XRD analysis and are presented in Figure S2 of the Supporting Information [orthorhombic phase for GaO(OH)

DOI: 10.1021/acs.energyfuels.6b01568
Energy Fuels 2016, 30, 7419−7427

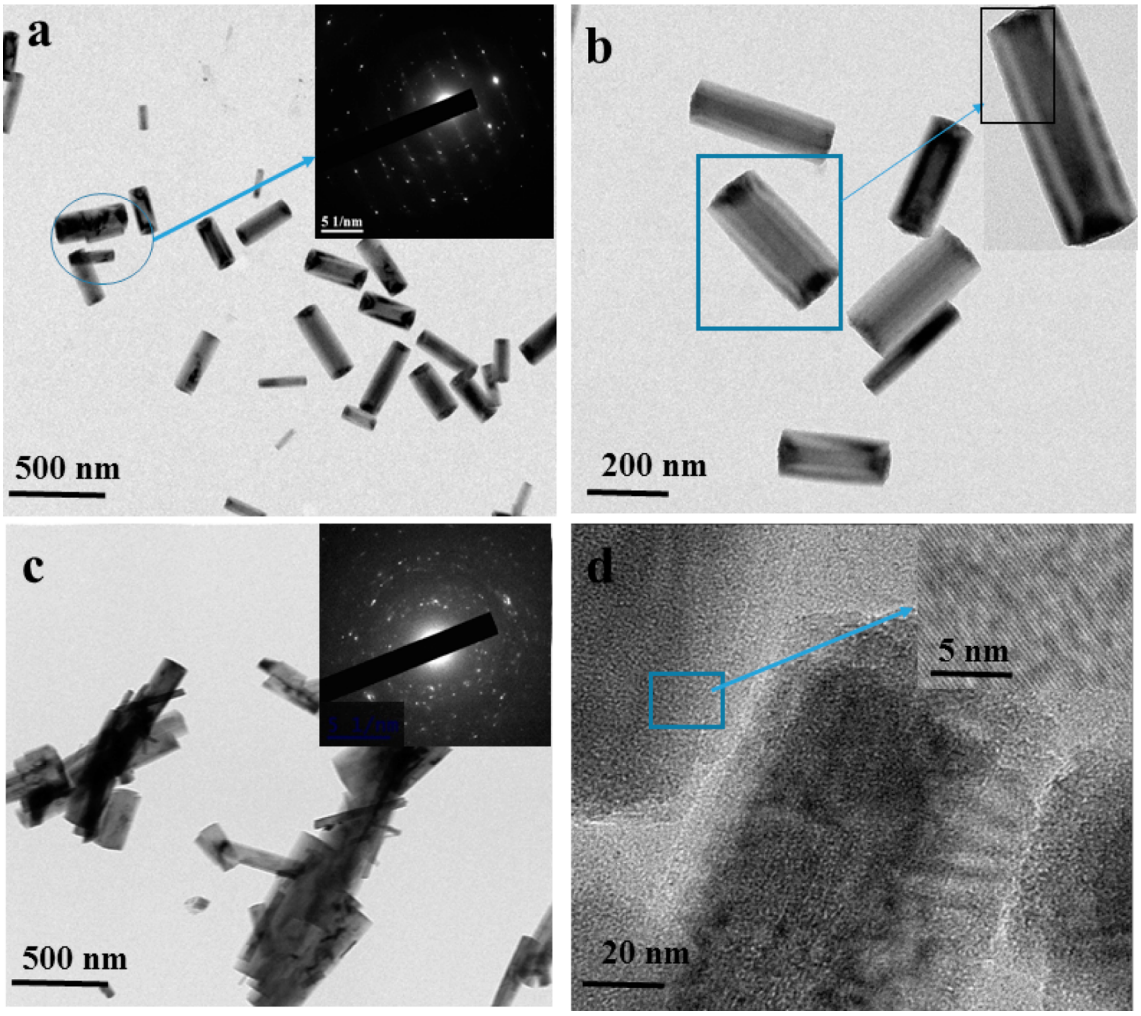

Figure 2. TEM images of (a) α-GaO(OH) (inset: SAED), (b) α-GaO(OH) (inset: magnified image of a single particle), and (c) β-Ga_2O_3 (inset: SAED) and (d) HRTEM images of β-Ga_2O_3 (inset: well-resolved lattice fringes).

and monoclinic phase for β-Ga_2O_3]. TEM and high-resolution transmission electron microscopy (HRTEM) images of α-GaO(OH) crystallites (after sonication of the molten Ga) are shown in panels a and b of Figure 2. The inset in Figure 2a shows the selected area electron diffraction (SAED) pattern of α-GaO(OH) with an orthorhombic crystal structure. Detailed analysis of the crystal structure was reported elsewhere.[15] A TEM image of the β-Ga_2O_3 crystallites is shown in Figure 2c, together with their SAED. The ring pattern reflects the polycrystalline nature of the β-Ga_2O_3 product. HRTEM images of the β-Ga_2O_3 particles are shown in Figure 2d. The observed d-spacing value for β-Ga_2O_3 is 0.36 nm, which fits well with the spacing of the monoclinic phase of the β-Ga_2O_3 plane. The elemental composition of the calcined product was also examined by energy-dispersive spectroscopy (EDS) (Figure S3 of the Supporting Information), and the presence of Ga and O without any impurities was confirmed (Figure S3 of the Supporting Information). Two elements observed on the spectrum, C and Cu, originated from the copper grid and the carbon tape, respectively.

Characteristic UV absorption bands were observed at 210 and 256 nm for α-GaO(OH) and β-Ga_2O_3, respectively (Figure S4a of the Supporting Information). α-GaO(OH) displayed no obvious absorbance at wavelengths up to 210 nm, indicating high transparency under UV light. For further conformation, we have used diffused reflectance spectroscopy. Both of these techniques, namely, UV−vis and diffused reflectance spectroscopy, use UV−vis light excited valence electrons to empty orbitals. The difference in these techniques is that, in UV−vis spectroscopy, the relative change of transmittance of light is measured as it passes through a solution, whereas in diffuse reflectance, the relative change in the amount of light reflected off a surface is examined. Analogous to the UV−vis spectra, a typical reflectance band is observed at 211 nm in the case of α-GaO(OH) and at 256 nm in the case of Ga_2O_3.

Furthermore, dynamic light scattering (DLS) and ζ potential measurements were performed to probe the surface charge and particle size distribution of the α-GaO(OH) and β-Ga_2O_3 nanorods. The α-GaO(OH) nanorods exhibit a ζ potential of −40.4 mV (Figure S5a of the Supporting Information) and a homogeneous size distribution. The hydrodynamic diameter of α-GaO(OH) decreases from 460 to 110 nm with the increase in the temperature from 25 to 50 °C (panels a and b of Figure 3).

At 20 °C, the hydrodynamic diameter of the β-Ga_2O_3 nanorods was about 480 nm with a corresponding ζ potential of −41.7 mV (Figure S5b of the Supporting Information), which is similar to the length of the β-Ga_2O_3 nanorods obtained in the corresponding TEM images (panels c and d of Figure 2). DLS measurements reveal a hydrodynamic diameter

DOI: 10.1021/acs.energyfuels.6b01568
Energy Fuels 2016, 30, 7419−7427

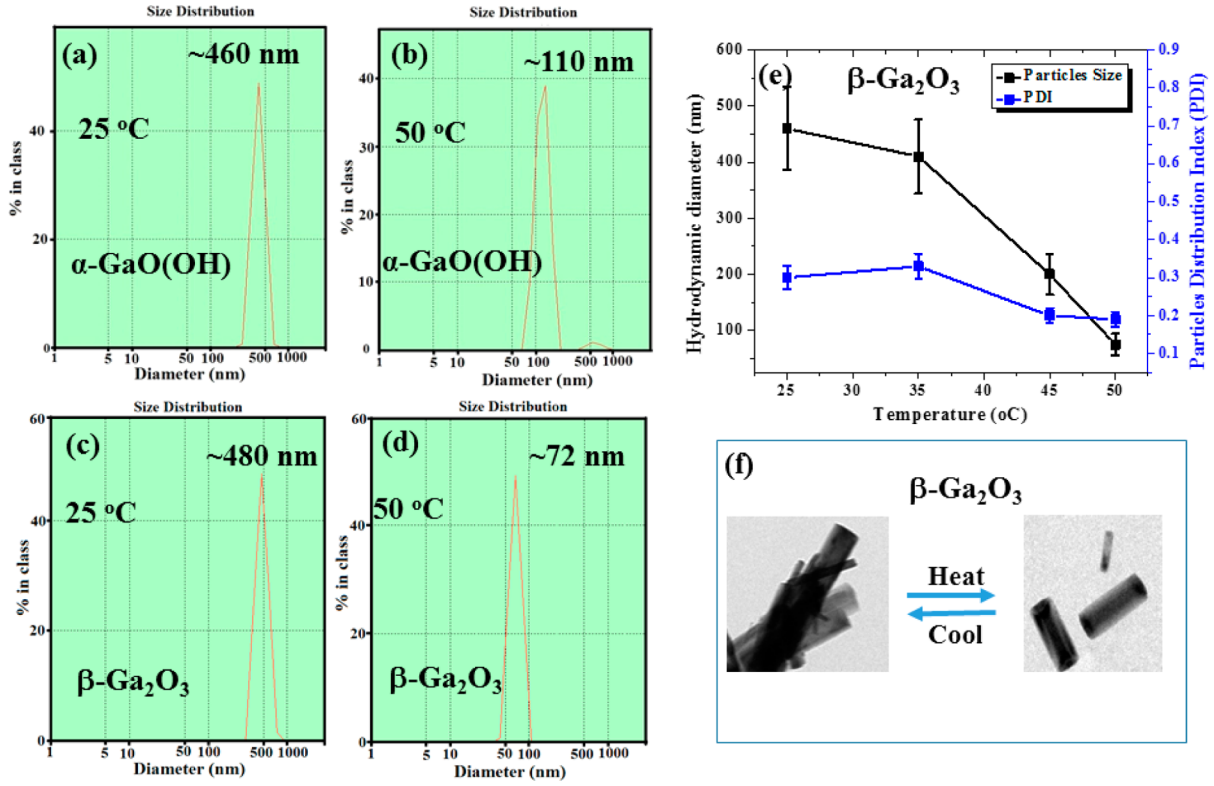

Figure 3. DLS curve of α-GaO(OH) at (a) 25 °C and (b) 50 °C, DLS plot of β-Ga_2O_3 at (c) 25 °C and (d) 50 °C, (e) hydrodynamic size versus temperature, and (f) speculation of coagulation and decoagulation of β-Ga_2O_3 nanorods.

of 480 nm for β-Ga_2O_3 at 25 °C and 72 nm at 50 °C (panels c and d of Figure 3). There is a sharp decline in the hydrodynamic size of β-Ga_2O_3 at temperatures above 35 °C (Figure 3e). At 50 °C, the corresponding hydrodynamic diameter of the β-Ga_2O_3 nanorods is only 72 nm. The particles exhibit a homogeneous dispersion with a particle distribution index (PDI) of ~0.25. The stability and speculated structure is shown in Figure 3f.

3.2. Dehydration of Xylose to Furfural by β-Ga_2O_3. Furfural was obtained from the dehydration of three water molecules dissociated from xylose by either liquid or solid acid catalysts.[26,27] The use of Ga_2O_3 as a catalyst helps to solve safety problems, such as the handling of strong acids, equipment corrosion, and waste treatment associated with strong acids. The reaction was carried out in an aqueous solution of xylose (0.17 M) at 150 °C for 12 h, and the formation of furfural was analyzed by ^{13}C NMR (Figure 4a). Thermosensitive Ga_2O_3 nanorods should have a small particle size and high surface area at this high temperature. As mentioned above, GaO(OH) can also catalyze this reaction. However, an appreciable amount of byproducts, including lactic acid, were detected when GaO(OH) was used as the catalyst. The reduced selectivity of GaO(OH) may be due to the basic sites (OH) present in this catalyst that promote the formation of lactic acid and other dehydration products. Nevertheless, furfural was formed with GaO(OH) as a result of the presence of the Ga^{3+} Lewis acid. Furfural and other byproducts were further analyzed by ^1H NMR in corroboration with the ^{13}C NMR results (Figure S6 of the Supporting Information). Consequently, a series of experiments was conducted using Ga_2O_3 to probe its loading effect. The amount of catalyst was varied between 0.5 and 0.1 g when dehydrating D-xylose (25 mg/mL) at 150 °C for 12 h. Both ^{13}C and ^1H NMR confirm

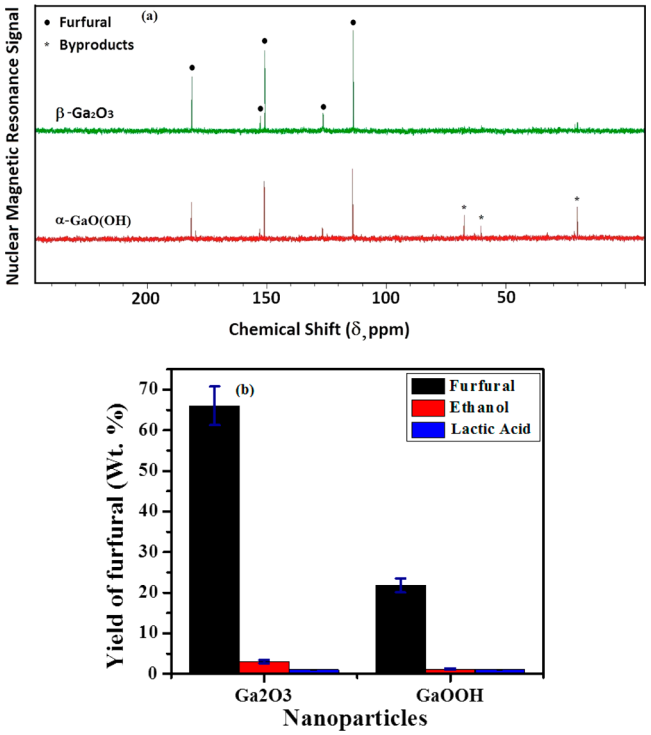

Figure 4. (a) ^{13}C NMR spectra of the product obtained from the hydrothermal reaction (12 h and 150 °C) with α-GaO(OH) and with β-Ga_2O_3 and (b) HPLC evaluation of α-GaO(OH) and β-Ga_2O_3 of the hydrolysate from D-xylose [conditions: 20 mL of neutral hydrolysate, 0.5 g of D-xylose, and 0.2 g of catalyst at 150 °C for 12 h; replicates of n = 3; error bars indicate standard deviation (SD)].

DOI: 10.1021/acs.energyfuels.6b01568
Energy Fuels 2016, 30, 7419−7427

Scheme 1. Proposed Reaction Mechanism for the Conversion of Xylose to Furfural Using β-Ga_2O_3 as a Catalyst

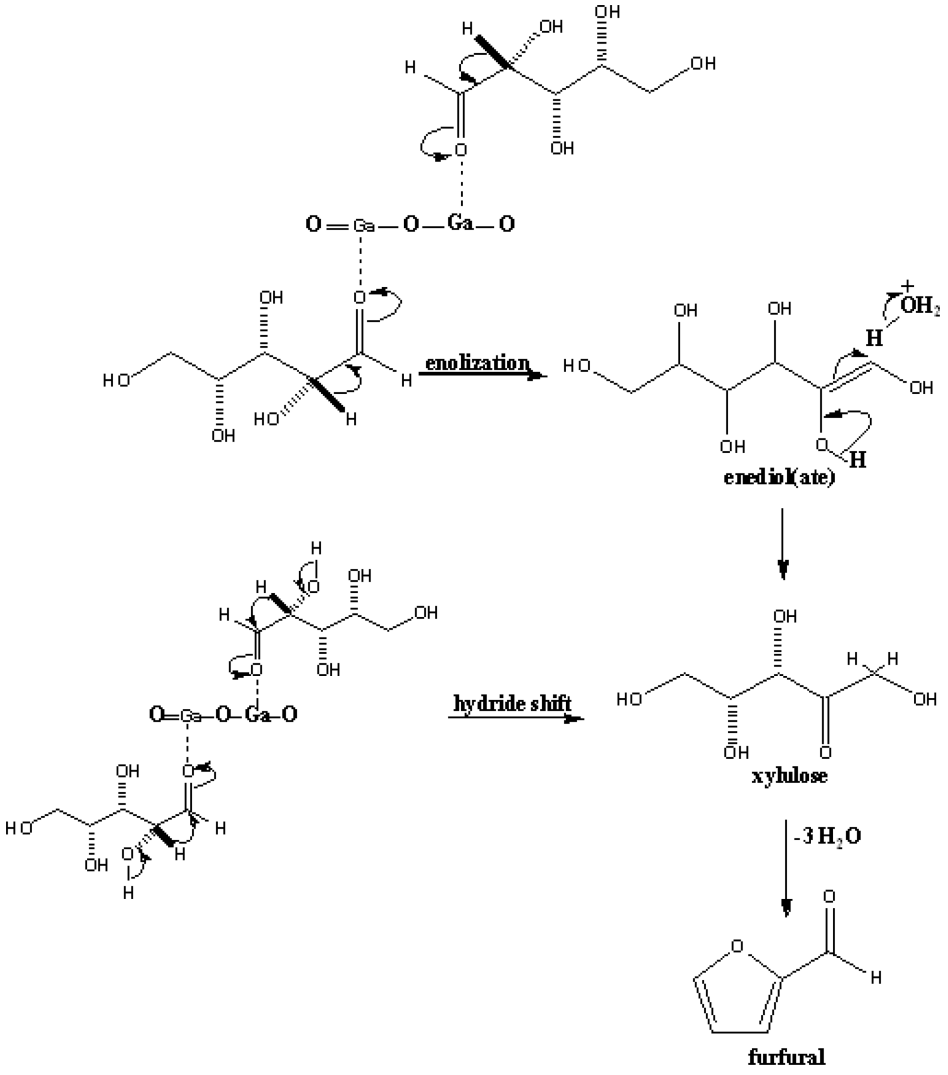

that the reaction was completed with a catalyst/xylose ratio of 1:1 and 0.4:1 (wt %) (Figure S7 of the Supporting Information). With further probing into the nature of the catalyst/xylose ratio (at lower ratios, 0.2:1 weight ratio), unreacted xylose was still detected after 12 h. Thus, 1:1 and 0.4:1 (wt %) (β-Ga_2O_3/xylose) ratios produce a high amount of furfural with higher selectivity than the 0.2:1 (wt %) (β-Ga_2O_3/xylose) ratio. As a result, the β-Ga_2O_3/xylose ratio of 0.4:1 (wt %) is chosen as the optimum, because this lower amount of β-Ga_2O_3 enables high furfural production.

The quantification of the furfural product was performed using HPLC analysis. As shown in Figure 4b, Ga_2O_3 is more active and selective for the dehydration of xylose to furfural than α-GaO(OH). The superiority of Ga_2O_3 is also reflected in the absence of any appreciable amount of byproducts, and the yield of furfural approaches 66 wt %. The selectivity toward the production of furfural reaches 94 and 30% for β-Ga_2O_3 and α-GaO(OH) catalysts, respectively. The yield obtained using β-Ga_2O_3 is compared to that obtained using Nafion 117, which hydrates xylose in dimethyl sulfoxide at 150 °C with only 60% of the theoretical furfural yield.[45] Similarly, sulfonated graphene oxide (SGO) can be used for the dehydration of xylose to furfural in water with an average yield of 61%.[46] No reactive oxygen species (ROS) are expected to be involved in this reaction because Ga_2O_3 does not produce ROS under room light.[47] Our previous study shows that blue light induces hydroxyl radical formation in Ga_2O_3, which is irrelevant to the current study.[47]

3.3. Postulated Dehydration Mechanism. Incomplete coordination of metal cations and oxide anions on the MO crystals facilitates the formation of acidic and basic sites on its surface. Thus, ionic MO surfaces are expected to contain coordinative unsaturated cations (Lewis acid sites) and basic sites. These Lewis acid sites that are exposed at the surface of the ionic oxides present a good opportunity for xylose (reducing sugar) to donate an electron to the metal cation to catalyze the reaction. Ga has an oxidation state of +3 in both Ga_2O_3 and GaO(OH). We adopted a mechanism consistent with the previous findings[48,49] that Ga^{3+} catalyzes the dehydration of xylose through a 1,2-hydride shift. Being a Lewis acid, Ga^{3+} carries the reaction in the forward direction by converting emerging xylose into an oxocarbenium ion. At the final stage, the deprotonation of this species results in enol, and the subsequent loss of three water molecules produces furfural. The proposed reaction scheme is presented in Scheme 1.

The higher yield of furfural that was obtained with Ga_2O_3 (66%), in comparison to GaO(OH) (22%), as illustrated in the HPLC results, can be explained by considering the role of the

DOI: 10.1021/acs.energyfuels.6b01568
Energy Fuels 2016, 30, 7419−7427

Lewis acid sites in the catalysis. Ga_2O_3 have two Ga atoms per molecule, whereas GaO(OH) has only one Ga atom per molecule. Because the catalytic activity is attributed to the Ga^{3+} ions, two Ga atoms provide a greater probability for D-xylose molecules to react on its surface and carry out the reaction in the forward direction than in the case of GaO(OH). Brunauer–Emmett–Teller (BET) also showed a higher surface area (17 m^2/g) for Ga_2O_3 than for GaO(OH) (10 m^2/g). The increased surface area also promotes a strong interaction between xylose and Ga_2O_3 compared to GaO(OH).

After the dehydration of xylose to furfural, used Ga_2O_3 was separated from the reaction liquid and subjected to XRD analysis (Figure 5). The XRD pattern of used Ga_2O_3 was

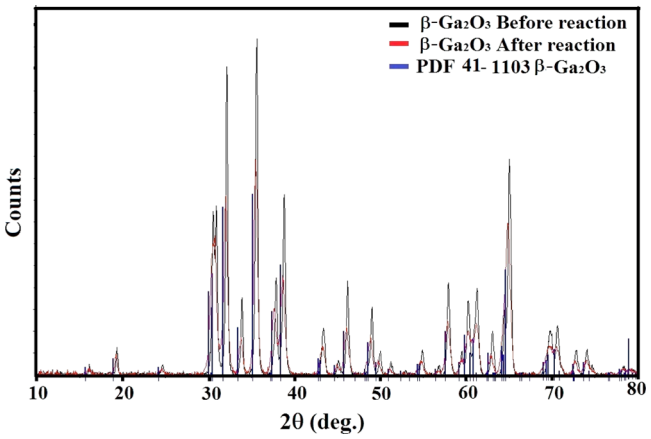

Figure 5. XRD pattern of the β-Ga_2O_3 catalyst before and after the reaction.

virtually identical to that of pristine Ga_2O_3. Moreover, SEM and TEM analyses were also carried out to probe the morphology of the used catalyst. No morphological changes were observed in the catalyst before and after the reaction (Figure S8 of the Supporting Information). Such a result provides a reason for the reuse of this solid catalyst and its application in a packed/fluidized-bed reactor for continuous processing and facilitated furfural recovery.

3.4. Reusability Study of the β-Ga_2O_3 Catalyst. β-Ga_2O_3 was reused to demonstrate the reusability of the catalyst for the production of furfural, and a similar result to that of freshly prepared β-Ga_2O_3 was obtained. The reusability of β-Ga_2O_3 was tested for three reaction runs under optimal reaction conditions. To reduce the loss of catalyst material during separation and drying, the reaction product obtained in each case was separated from the catalyst by centrifugation. Fresh xylose and water were added to the residual solid that remained from the catalyst in the centrifugation tube. The contents were transferred to the hydrothermal reactor and subjected to 150 °C for 12 h. The effective reusability of β-Ga_2O_3 was attributed to its good crystalline structure. The reaction products obtained from each of the three reaction runs were analyzed by ^{13}C NMR (Figure S9 of the Supporting Information). Peaks characteristic of furfural alone were observed in the hydrolysate after two regenerations of the catalyst. Moreover, the xylose conversion was complete. Thus, a reusable, active, and selective catalyst for the hydrolysis of xylose to furfural has been designed. Because the current process of furfural production from xylose uses β-Ga_2O_3 at modest loadings (0.4:1 β-Ga_2O_3/xylose ratio), a simple and surfactant-free catalyst is relatively cheap. In addition, the use of β-Ga_2O_3 facilitates the selective production of furfural from xylose. Because of the special features of this catalytic process, it can be used for industrial purposes.

4. CONCLUSION

A novel surfactant-free, acid-base free sonochemical pathway for the preparation of Ga_2O_3 nanorods from molten Ga metal is reported. Combined sonication and calcination shortens the duration of the catalyst preparation (6 h) compared to conventional wet impregnation techniques. The β-Ga_2O_3 catalyst exhibits good activity and selectivity in the conversion of xylose to furfural, which resulted in 94% yield of furfural with 66 wt % selectivity in 12 h at 150 °C. This catalyst was observed to be thermosensitive, which might be a key factor leading to higher production of furfural from xylose. This solid catalyst can be easily separated from the product and reused for the conversion of biomass to important platform chemicals. The detailed mechanism of the conversion of D-xylose to furfural is proposed. The chemical and thermosensitive behavior of the catalyst under the reaction conditions make it a reusable and potential catalytic system for industrial application in producing furfural from xylose. It is desirable to probe further into the kinetics of the process by measuring the rate of the reaction. These studies are now in progress.

■ ASSOCIATED CONTENT

Supporting Information

The Supporting Information is available free of charge on the ACS Publications website at DOI: 10.1021/acs.energyfuels.6b01568.

HRSEM, EDS, TEM, NMR, UV–vis, and XRD investigations of the catalyst and products (PDF)

■ AUTHOR INFORMATION

Corresponding Author

*Telephone: 972-3-5318-315. Fax: 972-3-73804053. E-mail: gedanken@mail.biu.ac.il.

Author Contributions

†Vijay Bhooshan Kumar and Rahul Kumar Mishra contributed equally to this work.

Notes

The authors declare no competing financial interest.

■ ACKNOWLEDGMENTS

Aharon Gedanken thanks the Israel Ministry of Science and Technology for the Research Grant 3-99763 and the Israel Science Foundation for supporting the research via Grant 598/12.

■ REFERENCES

(1) De, B.; Voit, B.; Karak, N. Carbon Dot Reduced Cu_2O Nanohybrid/hyperbranched Epoxy Nanocomposite: Mechanical, Thermal and Photocatalytic Activity. *RSC Adv.* **2014**, *4*, 58453–58459.

(2) Shen, L.; Chen, M.; Hu, L.; Chen, X.; Wang, J. Growth and Stabilization of Silver Nanoparticles on Carbon Dots and Sensing Application. *Langmuir* **2013**, *29*, 16135–16140.

(3) Liu, X.; Zhang, J.; Wang, L.; Yang, T.; Guo, X.; Wu, S.; Wang, S. 3D Hierarchically Porous ZnO Structures and Their Functionalization by Au Nanoparticles for Gas Sensors. *J. Mater. Chem.* **2011**, *21*, 349.

(4) Yan, S.; Wan, L.; Li, Z.; Zhou, Y.; Zou, Z. Synthesis of a Mesoporous Single Crystal Ga_2O_3 Nanoplate with Improved Photo-

DOI: 10.1021/acs.energyfuels.6b01568
Energy Fuels 2016, 30, 7419–7427

luminescence and High Sensitivity in Detecting CO. *Chem. Commun. (Cambridge, U. K.)* **2010**, *46*, 6388−6390.
(5) Liu, Z.; Yamazaki, T.; Shen, Y.; Kikuta, T.; Nakatani, N.; Li, Y. O_2 and CO Sensing of Ga_2O_3 Multiple Nanowire Gas Sensors. *Sens. Actuators, B* **2008**, *129*, 666−670.
(6) Arnold, S. P.; Prokes, S. M.; Perkins, F. K.; Zaghloul, M. E. Design and Performance of a Simple, Room-Temperature Ga_2O_3 Nanowire Gas Sensor. *Appl. Phys. Lett.* **2009**, *95*, 103102.
(7) Muruganandham, M.; Amutha, R.; Wahed, M. S. M. A.; Ahmmad, B.; Kuroda, Y.; Suri, R. P. S.; Wu, J. J.; Sillanpää, M. E. T. Controlled Fabrication of α-GaOOH and α-Ga 2O 3 Self-Assembly and Its Superior Photocatalytic Activity. *J. Phys. Chem. C* **2012**, *116*, 44−53.
(8) Hegde, M.; Hosein, I. D.; Radovanovic, P. V. Molecular Origin of Valence Band Anisotropy in Single β-Ga_2O_3 Nanowires Investigated by Polarized X-Ray Absorption Imaging. *J. Phys. Chem. C* **2015**, *119*, 17450−17457.
(9) Li, Z.; de Groot, C.; Moodera, J. H. Gallium Oxide as an Insulating Barrier for Spin-Dependent Tunneling Junctions. *Appl. Phys. Lett.* **2000**, *77*, 3630.
(10) Muruganandham, M.; Suri, R.; Abdel Wahed, M. S. M.; Sillanpää, M.; Ahmmad, B.; Lee, G. J.; Wu, J. J. Solvothermal Synthesis of Mesoporous α-GaOOH Semi-Nanospheres. *Mater. Lett.* **2013**, *111*, 137−139.
(11) Zhang, J.; Liu, Z.; Lin, C.; Lin, J. A Simple Method to Synthesize β-Ga_2O_3 Nanorods and Their Photoluminescence Properties. *J. Cryst. Growth* **2005**, *280*, 99−106.
(12) Huang, C. C.; Yeh, C. S.; Ho, C. J. Laser Ablation Synthesis of Spindle-like Gallium Oxide Hydroxide Nanoparticles with the Presence of Cationic Cetyltrimethylammonium Bromide. *J. Phys. Chem. B* **2004**, *108*, 4940−4945.
(13) Xiao, H. Di; Ma, H. L.; Liang, W.; Xue, C. S.; Zhuang, H. Z.; Ma, J.; Hu, W. R. GaO_2H, α-Ga_2O_3 and β-Ga_2O_3 Powders Synthesized from Ball-Milled GaN Powders. *Mater. Chem. Phys.* **2005**, *94*, 261−265.
(14) Patra, C. R.; Mastai, Y.; Gedanken, A. Microwave − Assisted Synthesis of Submicrometer GaO(OH) and Ga_2O_3 Rods. *J. Nanopart. Res.* **2004**, *6*, 509−518.
(15) Kumar, V. B.; Gedanken, A.; Porat, Z. Facile Synthesis of Gallium Oxide Hydroxide by Ultrasonic Irradiation of Molten Gallium in Water. *Ultrason. Sonochem.* **2015**, *26*, 340−344.
(16) Huang, X. D.; Lai, P. T.; Sin, J. K. O. Charge-Trapping Characteristics of Ga_2O_3 Nanocrystals for Nonvolatile Memory Applications. *ECS Solid State Lett.* **2012**, *1*, Q45−Q47.
(17) Zhu, C. H.; Hai, Z. B.; Cui, C. H.; Li, H. H.; Chen, J. F.; Yu, S. H. In Situ Controlled Synthesis of Thermosensitive poly(*N*-Isopropylacrylamide)/Au Nanocomposite Hydrogels by Gamma Radiation for Catalytic Application. *Small* **2012**, *8*, 930−936.
(18) Yin, T.; Liu, X.; Wang, J.; An, Y.; Zhang, Z.; Shi, L. Thermosensitive Mixed Shell Polymeric Micelles Decorated with Gold Nanoparticles at the Outmost Surface: Tunable Surface Plasmon Resonance and Enhanced Catalytic Properties with Excellent Colloidal Stability. *RSC Adv.* **2015**, *5*, 47458−47465.
(19) Liu, G.; Wang, D.; Zhou, F.; Liu, W. Electrostatic Self-Assembly of Au Nanoparticles onto Thermosensitive Magnetic Core-Shell Microgels for Thermally Tunable and Magnetically Recyclable Catalysis. *Small* **2015**, *11*, 2807−2816.
(20) Han, J.; Liu, Y.; Guo, R. Reactive Template Method to Synthesize Gold Nanoparticles with Controllable Size and Morphology Supported on Shells of Polymer Hollow Microspheres and Their Application for Aerobic Alcohol Oxidation in Water. *Adv. Funct. Mater.* **2009**, *19*, 1112−1117.
(21) Agirrezabal-Telleria, I.; Gandarias, I.; Arias, P. L. Heterogeneous Acid-Catalysts for the Production of Furan-Derived Compounds (Furfural and Hydroxymethylfurfural) from Renewable Carbohydrates: A Review. *Catal. Today* **2014**, *234*, 42−58.
(22) Brazdausks, P.; Puķe, M.; Vedernikovs, N.; Krüma, I. The Effect of Catalyst Amount on the Production of Furfural and Acetic Acid from Birch Wood in a Biomass Pretreatment Process. *Balt. For.* **2014**, *20*, 106−114.
(23) Patarin, J. Mild Methods for Removing Organic Templates from Inorganic Host Materials. *Angew. Chem., Int. Ed.* **2004**, *43*, 3878−3880.
(24) Tanabe, K. Industrial Application of Solid Acid−base Catalysts. *Appl. Catal., A* **1999**, *181*, 399−434.
(25) Branca, C.; Di Blasi, C.; Galgano, A. Catalyst Screening for the Production of Furfural from Corncob Pyrolysis. *Energy Fuels* **2012**, *26*, 1520−1530.
(26) Marcotullio, G.; De Jong, W. Chloride Ions Enhance Furfural Formation from D-Xylose in Dilute Aqueous Acidic Solutions. *Green Chem.* **2010**, *12*, 1739−1746.
(27) Lima, S.; Neves, P.; Antunes, M. M.; Pillinger, M.; Ignatyev, N.; Valente, A. A. Conversion of Mono/di/polysaccharides into Furan Compounds Using 1-Alkyl-3-Methylimidazolium Ionic Liquids. *Appl. Catal., A* **2009**, *363*, 93−99.
(28) Mandalika, A.; Runge, T. Enabling Integrated Biorefineries through High-Yield Conversion of Fractionated Pentosans into Furfural. *Green Chem.* **2012**, *14*, 3175−3184.
(29) Rong, C.; Ding, X.; Zhu, Y.; Li, Y.; Wang, L.; Qu, Y.; Ma, X.; Wang, Z. Production of Furfural from Xylose at Atmospheric Pressure by Dilute Sulfuric Acid and Inorganic Salts. *Carbohydr. Res.* **2012**, *350*, 77−80.
(30) Serrano-Ruiz, J. C.; Campelo, J. M.; Francavilla, M.; Romero, A. a.; Luque, R.; Menéndez-Vázquez, C.; García, A. B.; García-Suárez, E. J. Efficient Microwave-Assisted Production of Furfural from C_5 Sugars in Aqueous Media Catalysed by Brönsted Acidic Ionic Liquids. *Catal. Sci. Technol.* **2012**, *2*, 1828.
(31) Moreau, C.; Durand, R.; Peyron, D.; Duhamet, J.; Rivalier, P. Selective Preparation of Furfural from Xylose over Microporous Solid Acid Catalysts. *Ind. Crops Prod.* **1998**, *7*, 95−99.
(32) Otomo, R.; Tatsumi, T.; Yokoi, T. Beta Zeolite: A Universally Applicable Catalyst for the Conversion of Various Types of Saccharides into Furfurals. *Catal. Sci. Technol.* **2015**, *5*, 4001−4007.
(33) Kim, S. B.; You, S. J.; Kim, Y. T.; Lee, S.; Lee, H.; Park, K.; Park, E. D. Dehydration of D-Xylose into Furfural over H-Zeolites. *Korean J. Chem. Eng.* **2011**, *28*, 710−716.
(34) Lima, S.; Pillinger, M.; Valente, A. A. Dehydration of D-Xylose into Furfural Catalysed by Solid Acids Derived from the Layered Zeolite Nu-6(1). *Catal. Commun.* **2008**, *9*, 2144−2148.
(35) Antunes, M. M.; Lima, S.; Fernandes, A.; Candeias, J.; Pillinger, M.; Rocha, S. M.; Ribeiro, M. F.; Valente, A. A. Catalytic Dehydration of D-Xylose to 2-Furfuraldehyde in the Presence of Zr-(W,Al) Mixed Oxides. Tracing by-Products Using Two-Dimensional Gas Chromatography-Time-of-Flight Mass Spectrometry. *Catal. Today* **2012**, *195*, 127−135.
(36) Chareonlimkun, A.; Champreda, V.; Shotipruk, A.; Laosiripojana, N. Catalytic Conversion of Sugarcane Bagasse, Rice Husk and Corncob in the Presence of TiO_2, ZrO_2 and Mixed-Oxide TiO_2−ZrO_2 under Hot Compressed Water (HCW) Condition. *Bioresour. Technol.* **2010**, *101*, 4179−4186.
(37) Russo, P. a.; Lima, S.; Rebuttini, V.; Pillinger, M.; Willinger, M.-G.; Pinna, N.; Valente, A. A. Microwave-Assisted Coating of Carbon Nanostructures with Titanium Dioxide for the Catalytic Dehydration of D-Xylose into Furfural. *RSC Adv.* **2013**, *3*, 2595.
(38) Chang, C.; MA, X.; CEN, P. Kinetics of Levulinic Acid Formation from Glucose Decomposition at High Temperature. *Chin. J. Chem. Eng.* **2006**, *14*, 708−712.
(39) Li, X.; Jiang, Y.; Wang, L.; Meng, L.; Wang, W.; Mu, X. Effective Low-Temperature Hydrolysis of Cellulose Catalyzed by Concentrated $H_3PW_{12}O_{40}$ under Microwave Irradiation. *RSC Adv.* **2012**, *2*, 6921.
(40) Pulidindi, I. N.; Kimchi, B. B.; Gedanken, A. Can Cellulose Be a Sustainable Feedstock for Bioethanol Production? *Renewable Energy* **2014**, *71*, 77−80.
(41) Peng, L.; Lin, L.; Zhang, J.; Zhuang, J.; Zhang, B.; Gong, Y. Catalytic Conversion of Cellulose to Levulinic Acid by Metal Chlorides. *Molecules* **2010**, *15*, 5258−5272.
(42) Kumar, V. B.; Koltypin, Y.; Gedanken, A.; Porat, Z. Ultrasonic Cavitation of Molten Gallium in Water: Entrapment of Organic Molecules in Gallium Microspheres. *J. Mater. Chem. A* **2014**, *2*, 1309.

DOI: 10.1021/acs.energyfuels.6b01568
Energy Fuels 2016, 30, 7419−7427

(43) Kumar, V. B.; Gedanken, A.; Kimmel, G.; Porat, Z. Ultrasonic Cavitation of Molten Gallium: Formation of Micro- and Nano-Spheres. *Ultrason. Sonochem.* **2014**, *21*, 1166−1173.
(44) Kumar, V. B.; Mastai, Y.; Porat, Z.; Gedanken, A. Chiral Imprinting in Molten Gallium. *New J. Chem.* **2015**, *39*, 2690−2696.
(45) Lam, E.; Majid, E.; Leung, A. C. W.; Chong, J. H.; Mahmoud, K. A.; Luong, J. H. T. Synthesis of Furfural from Xylose by Heterogeneous and Reusable Nafion Catalysts. *ChemSusChem* **2011**, *4*, 535−541.
(46) Lam, E.; Chong, J. H.; Majid, E.; Liu, Y.; Hrapovic, S.; Leung, A. C. W.; Luong, J. H. T. Carbocatalytic Dehydration of Xylose to Furfural in Water. *Carbon* **2012**, *50*, 1033−1043.
(47) Tzitrinovich, Z.; Lipovsky, A.; Gedanken, A.; Lubart, R. Visible Light-Induced OH Radicals in Ga_2O_3: An EPR Study. *Phys. Chem. Chem. Phys.* **2013**, *15*, 12977−12977.
(48) Saad, L.; Riad, M. Characterization of Various Zinc Oxide Catalysts and Their Activity in the Dehydration-Dehydrogenation of Isobutanol. *J. Serb. Chem. Soc.* **2008**, *73*, 997−1009.
(49) Binder, J. B.; Blank, J. J.; Cefali, A. V.; Raines, R. T. Synthesis of Furfural from Xylose and Xylan. *ChemSusChem* **2010**, *3*, 1268−1272.

DOI: 10.1021/acs.energyfuels.6b01568
Energy Fuels 2016, 30, 7419−7427